Baryon spectrum of the Skyrme model

Michael P. Mattis and Marek Karliner
Stanford Linear Accelerator Center, Stanford University, Stanford, California 94305
(Received 11 January 1985)

We calculate the spectrum of nucleon and Δ resonances of the Skyrme model. The masses that we find are accurate on the average to within 8% of their experimental values up to 3 GeV. For most partial waves the model reproduces many significant features of the experimental Argand diagrams correctly. The values of the Skyrme parameters obtained from a best fit to the spectrum improve some of the static properties of the model.

I. INTRODUCTION

Recent months have seen a flurry of work on the model first proposed by Skyrme nearly a quarter of a century ago.[1] This model is just one particular choice for a nonlinear σ model describing the breakdown of the chiral symmetries $SU(2)_L \times SU(2)_R$ down to isospin. But it has the great advantage of being only second order in time derivatives, and hence, of succumbing to the traditional methods of Hamiltonian quantum mechanics. Furthermore, it possesses soliton solutions, or "Skyrmions," of finite extent. Thus the Skyrme model is an ideal testing ground for Witten's imaginative proposal[2,3] that—insofar as the "3" in $SU(3)_{\text{color}}$ can be considered a large number—baryons ought to emerge as solitons in the nonlinear σ model of the pion field.

In the framework of this model one can calculate many static properties of baryons such as magnetic moments, g factors, and charge radii.[4] Despite some glaring exceptions, these typically agree with experiment to within 30%, when the adjustable parameters of the model are chosen to give the nucleon and Δ masses correctly. Much less attention, however, has been focused on the dynamical properties of Skyrmions. Important progress in this direction was made independently by Zahed, Meissner, and Kaulfuss,[5] Breit and Nappi,[6] and Walliser and Eckart.[7] Interpreting fluctuations around the soliton as pion-nucleon scattering, the authors of Refs. 5 and 6 calculated the phase shifts in the "breathing mode"[8] of the Skyrmion and looked for a resonance in this channel by seeing if and when the phase shift crossed 90°. (We shall adopt a different criterion for the existence of a resonance below.) With this criterion there is no resonance for the case of massless pions, and a marginal resonance at 1270 MeV for massive pions, which Breit and Nappi identified with the real-world Roper resonance $P_{11}(1440)$. (We shall follow the standard notation $L_{2I,2J}$ for resonances, where $L = S,P,D,F,\ldots$ denotes the partial wave in which the resonance is formed, and I and J give the total isospin and angular momentum. Nucleon and Δ resonances are characterized by $I=\frac{1}{2}$ and $I=\frac{3}{2}$, respectively.) This work was greatly extended in the multiple-channel analysis of the group at Siegen University; we shall discuss their results at the end of this section.

In this spirit we have examined the processes $\pi N \to \pi N$ and $\pi N \to \pi\Delta$ in all channels of isospin and angular momentum for which experimental data was available for comparison. This paper can be viewed as a detailed application to one particularly tractable model of the more general considerations of Ref. 10; as such, it constitutes a lowest-order calculation in $1/N$, with N the number of colors of the underlying gauge group.

We are not motivated by the belief that there is anything especially fundamental about the Skyrme Lagrangian. Rather, we find it instructive to see how well the actual spectrum of nucleon and Δ resonances can be fit starting from a model that contains no explicit baryon fields and only three adjustable parameters. Indeed, in this paper we specialize to a two-parameter fit (one-parameter if the proton mass is fixed) by working in the chiral limit $m_\pi = 0$; the results of turning on a pion mass will be presented in a future publication.[9] Nevertheless our findings are in generally good agreement with the real world for energies up to 3 GeV, with resonance masses predicted on the average to within 8% of their actual values. (Our baryon-mass predictions are presented in Table I of Sec. III.) This is all the more surprising given the rather drastic nature of our approximations, such as completely neglecting baryon recoil. As a bonus we find that our "best fit" values for the Skyrme parameters substantially improve some of the static properties of the model.

Another noteworthy result of the Skyrme-model calculation concerns the qualitative behavior of the πN phase shifts in a given partial wave for adjacent values of J. Specifically, for each partial wave $L \geq 2$, the amplitude $L_{1,2L-1}$ moves much further in the unitarity circle than does $L_{1,2L+1}$; while in contrast, for the $I=\frac{3}{2}$ channels, it is $L_{3,2L+1}$ that dominates $L_{3,2L-1}$. And in fact, with a surprisingly high degree of regularity, this is what one finds in Nature. Moreover, in the model as in Nature, this pattern becomes more and more pronounced with higher and higher L.

We should at the outset mention some of our disappointments as well. The most obvious of these is our failure to find in pion-Skyrmion scattering what in the real world is the most spectacular baryon resonance of all, the Δ itself; likewise the P_{11} and S_{31} channels at low energies are manifestly in poor agreement with experiment. It is not clear to us whether these represent failures of the

Skyrme model or merely of our approximations near threshold. Either way, we shall argue that these discrepancies are not necessarily fatal to the model by showing that small perturbations can easily restore the correct low-energy behavior in these channels. In particular, we can expect the Δ to reappear in the next order in $1/N$. One can even take the optimistic view that these chiral-soliton models provide precisely the right framework for understanding why some of the S-, P, and D-wave channels contain clear, low-lying resonances, while others, in stark contrast, are marked by repulsive behavior near threshold. We will return to a full discussion of these matters in Sec. III, where we take up pion-nucleon scattering, but first, in Sec. II, we lay the groundwork by examining the "elementary" processes in which a pion scatters elastically off an unrotated Skyrmion (as we shall review below, nucleons and Δ's should properly be identified with rotating solitons).

While in the process of writing up our results we have learned of similar work (albeit from a somewhat different theoretical outlook) carried out at Siegen University.[7,11,12] In particular, much of the development in Sec. II and Appendix A, which concerns such elementary processes, is similar to that of Ref. 7. Furthermore, Eq. (20) below, which we borrow from Ref. 10, is derived in a different manner in Ref. 12; this equation gives the prescription for expressing physical pion-nucleon scattering as a linear superposition of elementary processes. The Argand plots presented in Ref. 12 (for F-wave πN elastic scattering only) appear to be in good numerical agreement with our own. We thank Dr. Hayashi for bringing this work to our attention.

Finally we should note that, although we assemble all the necessary machinery in this paper for dealing with $\pi N \to \pi\Delta$, we have chosen for the sake of conciseness to limit our presentation here to the elastic case $\pi N \to \pi N$. We will present the analogous $\pi\Delta$ results in the very near future.

II. PION SCATTERING FROM UNROTATED SKYRMIONS

In order to motivate our approach we begin with a brief review of the Skyrme model, essentially following Ref. 4. The Skyrme Lagrangian with a chiral-symmetry-breaking mass term is given by

$$\mathscr{L}=\frac{f_\pi^2}{16}\mathrm{Tr}\partial_\mu U\,\partial^\mu U^\dagger+\frac{1}{32e^2}\mathrm{Tr}[(\partial_\mu U)U^\dagger,(\partial_\nu U)U^\dagger]^2 + \frac{f_\pi^2 m_\pi^2}{8}(\mathrm{Tr}U-2) \tag{1}$$

with

$$U=e^{i\boldsymbol{\pi}(\mathbf{x},t)\cdot\boldsymbol{\sigma}}\ .$$

Here f_π is the pion decay constant (186 MeV in the real world), m_π is the pion mass, and e is a new, dimensionless coupling constant peculiar to the model. The "small parameter" $1/N$ enters the Lagrangian through f_π and e, which behave like $N^{1/2}$ and $N^{-1/2}$ in the large-N limit, respectively.

It is easy to guess[1] that $\mathscr{L}$ as given admits a "hedgehog" soliton solution of the form

$$U_0=e^{iF(r)\hat{\mathbf{r}}\cdot\boldsymbol{\sigma}}\ . \tag{2}$$

Indeed, if we plug this ansatz into (1) and look at small fluctuations about the soliton

$$F(r)\hat{\mathbf{r}}\to F(r)\hat{\mathbf{r}}+\frac{2}{f_\pi}\boldsymbol{\pi}(\mathbf{x},t) \tag{3}$$

we obtain the Euler equation

$$(\hat{\mathbf{r}}\cdot\boldsymbol{\pi})[(\tilde{r}^2+8\sin^2F)F''+2\tilde{r}F'+4\sin 2F(F')^2 -\sin 2F-\frac{4}{\tilde{r}^2}\sin^2F\sin 2F-\tilde{m}_\pi^2\tilde{r}^2\sin F]=0\ , \tag{4}$$

where the derivatives are taken with respect to the dimensionless variable $\tilde{r}=ef_\pi r$ and $\tilde{m}_\pi=m_\pi/ef_\pi$. Field configurations of the form (2) are thus automatically stable against angular fluctuations $\boldsymbol{\pi}=a\hat{\boldsymbol{\theta}}+b\hat{\boldsymbol{\phi}}$. To render them stable against radial fluctuations as well, one requires the expression in square brackets to vanish, which gives the defining equation for $F(r)$. It can be shown that the boundary conditions $F(0)=\pi$ and $F(\infty)=0$ yield a configuration of baryon number (i.e., topological charge) unity, as desired.

The ansatz (2) is of course not the only choice available. In particular, isospin rotations of the form AU_0A^{-1} yield equally acceptable soliton solutions (while preserving the vacuum at infinity). Indeed, it turns out that in order to form solitonic states of definite spin and isospin (i.e., nucleons and deltas), one must take a superposition of all possible A's, weighted by appropriately chosen wave functions $\chi_{i_z s_z}(A)$. Straightforward Hamiltonian quantum mechanics in the "collective coordinates" A then yields for the nucleon and Δ masses[4]

$$\begin{aligned} m_N&=m_0+\gamma e^3 f_\pi(\tfrac{1}{2}\times\tfrac{3}{2})\ ,\\ m_\Delta&=m_0+\gamma e^3 f_\pi(\tfrac{3}{2}\times\tfrac{5}{2})\ , \end{aligned} \tag{5}$$

where m_0 is the mass of the "elementary" (i.e., unrotated) Skyrmion (approximately $36.5f_\pi/e$) and $\gamma\approx 4.7\times10^{-3}$.

This concludes our brief review of the Skyrme model; in the remainder of this section we put aside the issue of collective coordinates and focus purely on the question of pion scattering from elementary Skyrmions of the form (2). Explicit forms of the rather unwieldy differential operators involved are presented in Appendix A. The results for the S matrix that we obtain in this section will be reassembled in the next to yield the amplitudes for the physical processes $\pi N\to\pi N$.

We proceed in a straightforward manner, by enforcing the substitution (3) in the Skyrme Lagrangian (1). After integration by parts one obtains

$$S=-m_0+\int d^4x\,\pi^{i*}(\mathbf{x},t)\hat{L}_{ij}\pi^j(\mathbf{x},t)+O(\pi^3/f_\pi) \tag{6}$$

with $\hat{L}$ a complicated 3×3 matrix of second-order differential operators. (We are allowing complex pion fields as a convenience; this way we are spared from having to take real parts of spherical harmonics and of $e^{i\omega t}$ throughout.) Consistent with the "large-N" spirit that motivates the model we will henceforth drop all terms of cubic or higher order in the pion fields; these are damped

by powers of $f_\pi \sim N^{1/2}$. As a result, the equations of motion for the pion fields that we will derive will be linear ones.

We can make substantial progress by realizing that $\hat{L}$, complicated though it may be, preserves the symmetry $\mathbf{K}=\mathbf{I}(\text{pion})+\mathbf{L}(\text{pion})$. Explicitly,

$$(-i\epsilon_{ijk}r^i\partial_j\delta_{bc}+i\epsilon_{kbc})\hat{L}_{ba} - \hat{L}_{cb}(-i\epsilon_{ijk}r^i\partial_j\delta_{ba}-i\epsilon_{kba})=0 . \quad (7)$$

We can take advantage of this fact by expanding the pion field in terms of the vector spherical harmonics (here given in the $\{+,0,-\}$ basis)

$$\mathbf{\Pi}_L^{KK_z}=\begin{bmatrix} \langle L,1,K_z-1,1\,|\,K,K_z\rangle Y_{L,K_z-1}(\Omega) \\ \langle L,1,K_z,0\,|\,K,K_z\rangle Y_{L,K_z}(\Omega) \\ \langle L,1,K_z+1,-1\,|\,K,K_z\rangle Y_{L,K_z+1}(\Omega) \end{bmatrix} \quad (8)$$

which are states of definite $\mathbf{K}^2$ and K_z. Accordingly we plug

$$\boldsymbol{\pi}(\mathbf{x},t)=\sum_{K,K_z}[\psi_-^{KK_z}(r,t)\mathbf{\Pi}_{K-1}^{KK_z}(\Omega)+\psi_0^{KK_z}(r,t)\mathbf{\Pi}_K^{KK_z}(\Omega) +\psi_+^{KK_z}(r,t)\mathbf{\Pi}_{K+1}^{KK_z}(\Omega)] \quad (9)$$

into (6). Parity precludes the ψ_0's from mixing with the $\psi_\pm$'s; ψ_+ and ψ_- can mix in this model, however, as they do in Nature, where jumps of two units of pion angular momentum are allowed in the process $\pi N\to\pi\Delta$.

The angular integration can be performed, thanks to the identities

$$\nabla\cdot\mathbf{\Pi}_{K-1}^{KK_z}=-\frac{K-1}{r}\hat{\mathbf{r}}\cdot\mathbf{\Pi}_{K-1}^{KK_z}=-\frac{K-1}{r}\left[\frac{K}{2K+1}\right]^{1/2}Y_{KK_z},$$
$$\nabla\cdot\mathbf{\Pi}_{K+1}^{KK_z}=\frac{K+2}{r}\hat{\mathbf{r}}\cdot\mathbf{\Pi}_{K+1}^{KK_z}=-\frac{K+2}{r}\left[\frac{K}{2K+1}\right]^{1/2}Y_{KK_z}, \quad (10)$$
$$\nabla\cdot\mathbf{\Pi}_K^{KK_z}=\hat{\mathbf{r}}\cdot\mathbf{\Pi}_K^{KK_z}=0 .$$

We are left with

$$S=-m_0+\sum_{K,K_z}\int r^2dr\,\psi_0^{KK_z}(r,t)^*\hat{L}_0^K\psi_0^{KK_z}(r,t)+\sum_{K,K_z}\int r^2dr(\psi_-^{KK_z}(r,t)^*,\psi_+^{KK_z}(r,t)^*)\begin{bmatrix}\hat{L}_{--}^K & \hat{L}_{-+}^K \\ \hat{L}_{+-}^K & \hat{L}_{++}^K\end{bmatrix}\begin{bmatrix}\psi_-^{KK_z}(r,t) \\ \psi_+^{KK_z}(r,t)\end{bmatrix}, \quad (11)$$

where the $\hat{L}^K$'s are complicated second-order differential operators in r and t alone. We will refer to the 2×2 matrix of operators here as $\hat{\mathbb{L}}^K$ and the two-component column vector of wave functions as Ψ^K.

The determination of phase shifts now proceeds in a completely straightforward manner. The "normal-mode" equations to be solved are

$$\hat{L}_0^K[\psi_0^K(r)e^{i\omega t}]=0 \quad (12a)$$

and

$$\hat{\mathbb{L}}^K[\Psi^K(r)e^{i\omega t}]=0 \quad (12b)$$

for all ω; here we are assuming that $\hat{L}$ and $\hat{\mathbb{L}}$ have been chosen with care to be self-adjoint. By time-reversal invariance $\hat{L}$ and $\hat{\mathbb{L}}$ are real operators, so it suffices to consider the real radial wave functions that are regular (i.e., square-integrable) at the origin and integrate out past the point where the Skyrmion profile $F(r)$ is negligible. In this regime the theory is one of free pions, so ψ_0^K can be fit to

$$A(\omega)j_K(kr)+B(\omega)n_K(kr)$$

with

$$k=(\omega^2-m_\pi^2)^{1/2} .$$

(We follow Messiah[13] in our definitions of the spherical Bessel functions.) The S matrix in this channel is extracted by rewriting this as

$$\text{constant}\times[h_K^- - s_{KKK}(\omega)h_K^+] \quad (13)$$

yielding

$$s_{KKK}(\omega)=-(B+iA)^{-1}(B-iA) \quad (14)$$

which lies on the unit circle. (Following Ref. 10 we will adopt the notational convention $s_{KL'L}$, where L and L' refer to the incoming and outgoing angular momentum of the pion, respectively.)

The 2×2 case (12b) proceeds analogously. Near the origin for each $K\geq1$ there are two independent regular solutions Ψ_1^K and Ψ_2^K, which behave asymptotically as

$$\Psi_i^K\sim\begin{bmatrix}A_i(\omega)j_{K-1}(kr)+B_i(\omega)n_{K-1}(kr) \\ C_i(\omega)j_{K+1}(kr)+D_i(\omega)n_{K+1}(kr)\end{bmatrix}, \quad i=1,2 . \quad (15)$$

[The exception is the translational zero mode (19b) below; the second zero-energy solution which is well behaved at the origin blows up for large r.] If we work in the convenient basis in which the incoming pions are in pure $(K-1)$ waves or $(K+1)$ waves of orbital angular momentum, the 2×2 S matrices are given by

$$S_K\equiv\begin{bmatrix}s_{K,K-1,K-1} & s_{K,K-1,K+1} \\ s_{K,K+1,K-1} & s_{K,K+1,K+1}\end{bmatrix} =-\begin{bmatrix}B_1+iA_1 & D_1+iC_1 \\ B_2+iA_2 & D_2+iC_2\end{bmatrix}^{-1}\begin{bmatrix}B_1-iA_1 & D_1-iC_1 \\ B_2-iA_2 & D_2-iC_2\end{bmatrix} . \quad (16)$$

In the next section we shall show that the amplitudes for elastic πN scattering in the Lth partial wave are in fact linear superpositions of $s_{L-1,LL}$, s_{LLL}, and $s_{L+1,LL}$.

Note that S_K as given is correctly invariant under dif-

ferent choices of regular solutions $\Psi_1'=\alpha\Psi_1+\beta\Psi_2$ and $\Psi_2'=\gamma\Psi_1+\delta\Psi_2$. Furthermore it is trivial to prove that a matrix of the form $-M^{-1}M^*$ can be unitary if and only if it is also complex-symmetric, so that $s_{213}=s_{231}$, etc. This result, which follows generally from time-reversal invariance,[14] provides a useful check on one's numerical calculations. Accordingly we can parametrize S_K as

$$\begin{pmatrix} \eta_K^{\mathrm{D}} e^{2i\delta_{K,K-1,K-1}} & \eta_K^{\mathrm{OD}} e^{2i\delta_{K,K-1,K+1}} \\ \eta_K^{\mathrm{OD}} e^{2i\delta_{K,K-1,K+1}} & \eta_K^{\mathrm{D}} e^{2i\delta_{K,K+1,K+1}} \end{pmatrix}, \tag{17}$$

where the phase shifts and absorption parameters are constrained by unitarity to obey

$$\delta_{K,K-1,K-1}(\omega)+\delta_{K,K+1,K+1}(\omega)-2\delta_{K,K-1,K+1}(\omega) = (n+\tfrac{1}{2})\pi \tag{18a}$$

and

$$(\eta_K^{\mathrm{D}}(\omega))^2+(\eta_K^{\mathrm{OD}}(\omega))^2=1\ . \tag{18b}$$

(The superscripts D and OD here stand for diagonal and off-diagonal.)

We should mention the special case $K=0$, for which only the rightmost term in (9) exists; this is the breathing mode $\pi\propto\hat{\mathbf{r}}$ of the Skyrmion. In our notation the only nonvanishing component of the S matrix when $K=0$ is $s_{011}=e^{2i\delta_{011}}$. We further note that the zero modes corresponding to rotations and translations of the Skyrmion,

$$\Pi_1^{1m}(\Omega)F(r) \tag{19a}$$

and

$$\left[F'+\frac{2F}{r}\right]\Pi_0^{1m}(\Omega)+\sqrt{2}\left[\frac{F}{r}-F'\right]\Pi_2^{1m}(\Omega)\ , \tag{19b}$$

respectively, appear in the model as threshold bound states. These will play a crucial role in our later discussions.

Some further details of the above procedure, including explicit expressions for $\hat{L}_0^K$ and $\hat{L}^K$, are given in Appendix A. The results of our phase-shift analysis for the various S-matrix components $s_{KLL'}$ with $L,L'\leq 7$ are plotted in Figs. 1–6. We have restricted our numerical analysis in the present paper to the case $m_\pi=0$.

Figure 1 depicts the phase shifts δ_{KKK} graphed against pion energy ω, measured in units of ef_π. (This number should be thought of as lying somewhere between 700 and 900 MeV; we will take up this matter in Sec. III.) The absence of a resonance for $K=1$ is of course due to the presence in this channel of the rotational zero mode (19a). For $K>1$ the obvious trend is for the resonances to become broader and more massive with increasing K.

Figures 2, 3, and 4 present our results for the diagonal components of S_K. Clearly, for $L\geq 3$, the phase-shifts $\delta_{L-1,L,L}$ rise sooner than δ_{LLL}, and certainly much more dramatically than $\delta_{L+1,L,L}$. As a consequence, the location of the resonances in the corresponding channels of πN scattering can essentially be read off from Fig. 2(b). In contrast to $L\geq 3$ note the tepid behavior of δ_{011} and δ_{122} [Fig. 2(a)]. The former is the breathing mode; as for the latter, the weak rise, like that of δ_{111}, is due to mixing with the translational mode (19b).

Figures 5 and 6 present the corresponding graphs for the off-diagonal elements $s_{K,K+1,K-1}$. These describe processes in which the orbital angular momentum of the pion jumps by two units. By conservation of angular momentum these processes are only relevant to $\pi N\to\pi\Delta$, and so we defer discussion to the future.

At this point we should make a technical comment about how we determined the location of resonances. In principle it is unsatisfactory merely to find where the phase shift crosses 90°, due to the often significant effects of background. A much more reliable criterion is to look for a well-defined peak in the speed $|dS/d\omega|$ in those regions where the amplitude is curving counterclockwise in the Argand diagram. Surprisingly, for $s_{K,K+1,K+1}$ this occurs when the phase-shifts are approximately 45°. We turn now to our main topic of pion-nucleon scattering in the Skyrme model.

III. PION-NUCLEON SCATTERING

So far we have discussed the (linearized) equations of motion for pions moving in a fixed external Skyrmion background. To relate this to πN and $\pi\Delta$ scattering requires a little group theory, and we will now just quote the result derived in Refs. 12 and 10.

For a given pion energy a physical process $\pi N\to\pi N$ or $\pi N\to\pi\Delta$ can be completely specified by the following quantum numbers: total isospin I, incoming and outgoing pion angular momenta L and L', and total angular momentum J. In addition we will let R' stand for the representation of the final baryon, i.e., $R'=\frac{1}{2}$ for N and $R'=\frac{3}{2}$ for Δ. One can show that the S matrix for any such process is given by

$$S_{LL'R'IJ}(\omega)=\sum_K P_{LL'\frac{1}{2}R'IJK}\,s_{KLL'}(\omega)\ . \tag{20a}$$

Here $S_{KLL'}$ refers to the S matrix for pions scattering from elementary Skyrmions as discussed in the previous section, and the P symbols are defined by

$$P_{LL'RR'IJK}=(-1)^{R'-R}[(2R+1)(2R'+1)]^{1/2}(2K+1) \times \begin{Bmatrix} K & I & J \\ R' & L' & 1 \end{Bmatrix} \begin{Bmatrix} K & I & J \\ R & L & 1 \end{Bmatrix}. \tag{20b}$$

The index K stands for the vector $\mathbf{K}=\mathbf{I}(\text{pion})+\mathbf{L}(\text{pion})$ introduced earlier. Equation (20) can thus best be interpreted as the decomposition of "physical" $\pi N\to\pi N$ or $\pi N\to\pi\Delta$ scattering in terms of pion scattering from elementary Skyrmions, where each of these elementary processes is characterized by its own conserved value of K.

Note that Eq. (20) holds quite generally for any chiral-soliton model which admits a classical solution of the hedgehog form (2). It is analogous to the Wigner-Eckart theorem in that a large number of physical matrix elements are expressed in terms of a substantially smaller set of "reduced" matrix elements weighted by appropriate group-theoretical coefficients. One can carry the analogy further by finding those special linear combinations for which the model-dependent right-hand side of (20a) can-

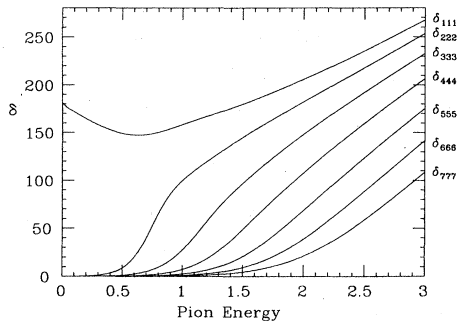

FIG. 1. Phase shifts δ_{KKK} plotted vs pion energy ω, measured in units of ef_π.

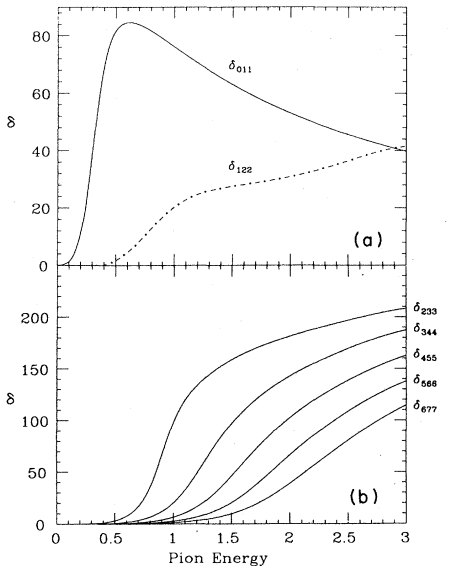

FIG. 2. Phase shifts $\delta_{K,K+1,K+1}$ plotted vs pion energy ω, measured in units of ef_π.

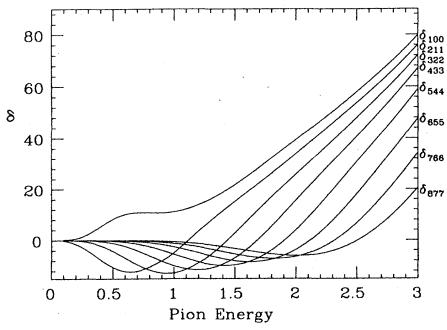

FIG. 3. Phase shifts $\delta_{K,K-1,K-1}$ plotted vs pion energy ω, measured in units of ef_π.

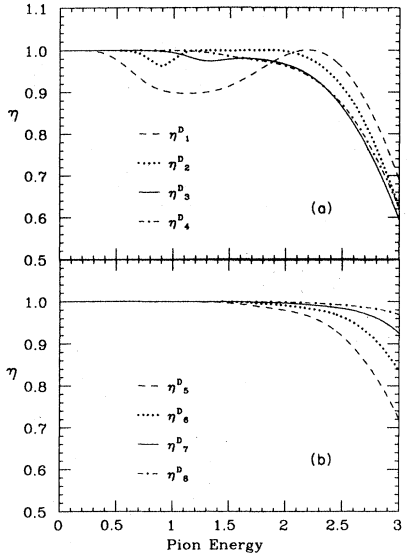

FIG. 4. Absorption parameters η_K^D plotted vs pion energy ω, measured in units of ef_π.

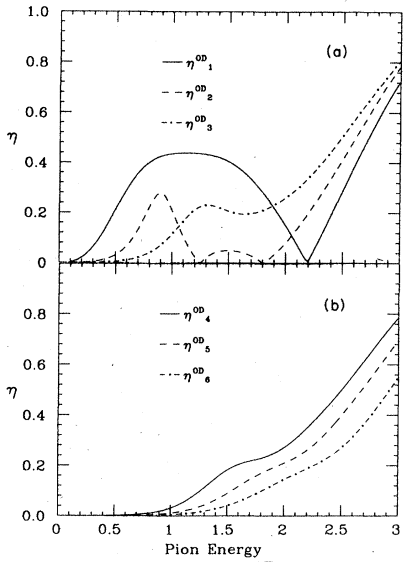

FIG. 5. Absorption parameters η_K^{OD} plotted vs pion energy ω, measured in units of ef_π.

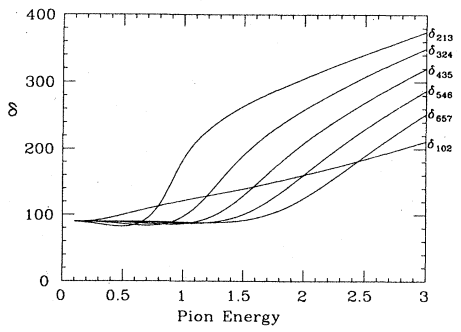

FIG. 6. Phase shifts $\delta_{K,K-1,K+1}$ plotted vs pion energy ω, measured in units of ef_π.

cels out; the net result will then be a set of energy-independent linear relations between physical scattering amplitudes that can serve as a test of the applicability of the chiral-soliton ansatz to the real world.[12,10] This program is carried out in detail in Ref. 10, with generally encouraging results.

We should point out, however, that the derivation of (20) requires the use of some fairly drastic approximations. For example, the collective coordinates characterizing the baryon are assumed not to change appreciably during the time of interaction, and, more seriously, baryon recoil is not taken into account. These approximations can be justified in the framework of the large-N expansion,[10] but in practice—where we would like to consider processes both near threshold and at pion energies on the order of the nucleon mass—they ought at least to make us wary.

Bearing this in mind, let us look at the implications of Eq. (20) for πN elastic scattering, which in our conventions means $R'=1/2$ and $L'=L$. The left-hand side of (20a) can then be reexpressed in the standard notation $L_{2I,2J}$, which we shall adopt from now on. From the explicit formulas for the relevant P symbols[10] we deduce

$$L_{1,2L-1}=\frac{2L-1}{3L}s_{L-1,L,L}+\frac{L+1}{3L}s_{LLL}\ , \tag{21a}$$

$$L_{1,2L+1}=\frac{L}{3L+3}s_{LLL}+\frac{2L+3}{3L+3}s_{L+1,L,L}\ , \tag{21b}$$

$$L_{3,2L-1}=\frac{(2L-1)(L-1)}{6L(2L+1)}s_{L-1,L,L}+\frac{2L-1}{6L}s_{LLL}+\frac{2L+3}{4L+2}s_{L+1,L,L}\ , \tag{21c}$$

$$L_{3,2L+1}=\frac{2L-1}{4L+2}s_{L-1,L,L}+\frac{2L+3}{6L+6}s_{LLL}+\frac{(L+2)(2L+3)}{6(L+1)(2L+1)}s_{L+1,L,L}\ . \tag{21d}$$

[Of course (21a) and (21c) only make sense if $L>0$; likewise the first term on the right-hand side of (21d) is absent for $L=0$]. Thus, for example, the P_{11} channel is given by $\frac{1}{3}s_{011}+\frac{2}{3}s_{111}$ instead of pure "breathing-mode" s_{011} as assumed in Refs. 5–7; this point was made in Ref. 12. We will return to this channel shortly.

The Argand plots obtained from these equations are presented in Fig. 8 of Appendix B, juxtaposed with the corresponding experimental results as drawn from Höhler *et al.*[15] (The experimental graphs are the "inner" ones.) As is customary we have graphed the T matrix instead of the S matrix; they are related by $T=(S-1)/2i$. Pion energy ω is given in units of ef_π for our graphs, while those drawn from Ref. 15 are parametrized by *total* center-of-mass energy W in GeV. For each of our resonances we give the corresponding value of ω, as well as the mass and width in MeV, using our "best-fit" values $\{e=4.79,\ f_\pi=150\ \text{MeV},\ ef_\pi=718.5\ \text{MeV}\}$ that we shall obtain at the end of this section.[16] The locations of resonances in the real-world data are indicated by vertical lines. Note that, as mentioned earlier, a resonance in the Skyrme model (as determined by the speed criterion) tends to occur toward the right-hand side of a circle and not at the top.

Before discussing the successes of the model we should confront its failures; these lie in the S and P waves. Indeed one's natural inclination is to turn first to the P_{33} channel, where in one of the cleanest examples of elastic scattering in Nature the Δ manifests itself dramatically as a full rotation around the unitarity circle. Instead, one finds in the Skyrme model initial *repulsive* (i.e., clockwise) behavior, followed by a highly inelastic resonance at $\omega\simeq 0.34ef_\pi$, then one that is extremely broad (and poorly defined) at $1.05ef_\pi$. A similar sad story, albeit somewhat less egregious, is to be found in the P_{11} channel; this is where the second-lightest resonance, the $N(1440)$, appears in Nature.

Yet these results are not necessarily fatal for the model. That is, despite the large discrepancies, one can argue that small perturbations in the P-wave sector of the theory can cause enormous effects in the corresponding Argand plots which could easily produce the observed real-world behavior for the amplitudes.

To see this, note that the physical P-wave amplitudes (P_{11} and P_{33} especially) all contain contributions from the elementary S-matrix element s_{111}, as is apparent from (21). This is the channel to which the rotational zero-mode of the Skyrmion, Eq. (19a), couples at threshold. As a result, in the model, the S matrix has a pole and a zero that have coalesced at the origin of the energy plane for all four P-wave channels of πN scattering. Now, one can easily envision effects which perturb these poles and zeros away from the origin; certainly the quantization of the collective coordinates, which involves the next order in the $1/N$ expansion, is one such effect. Consequently, some of these poles might end up in the fourth quadrant, slightly below the positive real axis [Fig. 7(a)], while others might be pushed into the second quadrant [Fig. 7(b)]. (These are quadrants of the "second sheet.")

If this scenario actually takes place in the real world, what would we actually observe? The channels in which the poles have been perturbed into the fourth quadrant would contain clear P-wave resonances lying reasonably close to threshold: suggestively, the resonances our model lacks, the $\Delta(1232)$ and the $N(1440)$, are in fact the two lowest-lying excitations in pion-nucleon scattering. In contrast, the channels in which the poles have been pushed into the first or second quadrant would be characterized by precisely the kind of *repulsive* behavior at low energies that one finds in the P_{13} and P_{31} amplitudes. Thus our scenario gives at least a consistent interpretation of the real-world P-wave amplitudes near threshold.

In a sense we already know that the Δ pole *must* be pushed into the fourth quadrant by such higher-order corrections. This, after all, is the essence of the calculation in Ref. 4 leading to the mass formula (5). Recall that in the large-N expansion $f_\pi\sim N^{1/2}$ while $e\sim N^{-1/2}$. Consequently, according to Eq. (5) (which of course gets renormalized by additional $1/N$ contributions), the nucleon-Δ mass difference is proportional to e^3f_π and hence of order $1/N$, whereas typical excitation energies as obtained in the present analysis are measured in units of ef_π which is of order unity. Thus it would actually have been inconsistent for the Δ to have appeared in our lowest-order calculation. [Note that the ratio

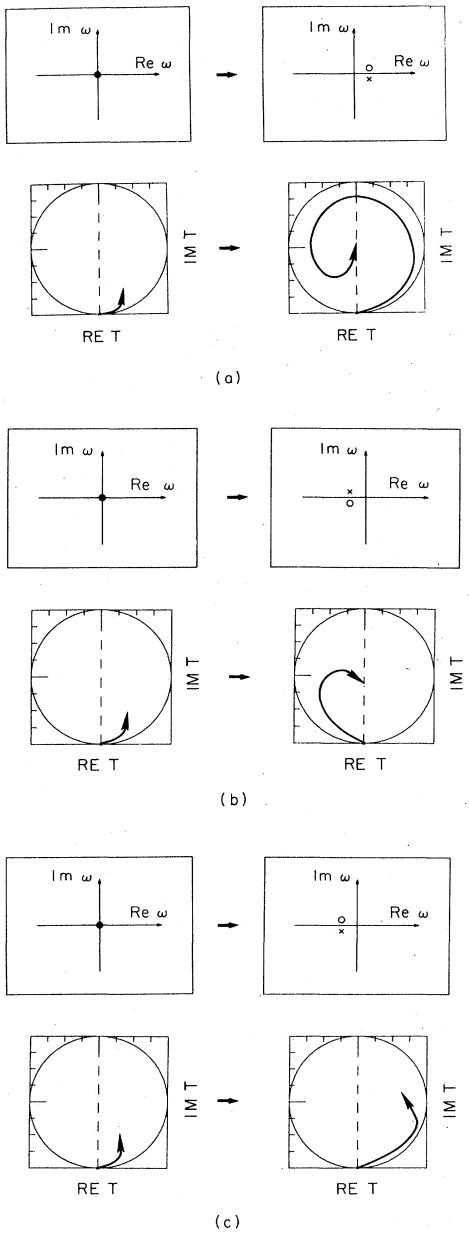

FIG. 7. Possible movement due to $1/N$ corrections of the poles and zeros of the S matrix in the complex energy plane, and the resulting effects on the amplitude near threshold. Poles are denoted by a cross and zeros by a circle.

$(m_\Delta - m_N)/m_N \sim 1/N^2$; this is just a special case of the well-known fact that the zero modes of a soliton, when quantized, produce energy splittings of order $\hbar^2$, which in the large-N approach is equivalent to $1/N^2$.]

Before leaving the P waves we ought to point out that the P_{13} and P_{31} amplitudes are already given quite nicely. [It is of course no coincidence that in the model $P_{31}=P_{13}$ and likewise $S_{31}=S_{13}$; this is a model-independent result that follows directly from Eq. (20).] Indeed the standard lore is that the repulsive regions of Argand diagrams are very difficult to concoct in quark models of resonances, and so we consider it especially satisfactory to find such behavior emerging automatically from such a simple model. Nor is the agreement merely qualitative: the "cusps" in the real-world P_{13} and P_{31} diagrams occur at 1530 and 1560 MeV, respectively, while the Skyrme-model prediction is 1640 MeV in each case.

We turn next to the S-wave channels, where we find a similar discrepancy. In particular the model fails to reproduce the observed initial repulsive behavior of the amplitude in the S_{31} channel. But the S waves couple to the *translational* modes of the soliton, Eq. (19b). Thus just as for the P waves one can argue that a small perturbation of the form depicted in Fig. 7(b) would induce such behavior. The situation for S_{11} is not so clear: If one considers the real-world resonance at 1526 MeV to be "close" to threshold then presumably it is Fig. 7(a) that gives the correct picture; otherwise it is Fig. 7(c).

In short, we have outlined a framework according to which all the S- and P-wave amplitudes in the real world can be understood as arising from higher-order corrections in an underlying chiral-soliton model such as Skyrme's. In particular, repulsive behavior near threshold arises in this picture from S-matrix poles that have been perturbed from the origin into the first or second quadrant. [Reassuringly, the only amplitude other than S_{31}, P_{31}, and P_{13} which exhibits such behavior in the real world is D_{35}, and this, too, mixes with the translational mode (19b).] Of course, at higher energies the effect of perturbing a threshold pole becomes negligible and so we would expect to see reasonable agreement once again between the model and experiment, as in fact we do in the S and P waves.

We turn now to the higher waves, which fortunately present no such problems. We can be brief since the graphs, for better or for worse, speak for themselves. By way of a conclusion we offer the following observations:

(1) The partial waves with $L \geq 2$ are on the whole in very satisfactory agreement with Nature. Many of the discrepancies in the higher waves can obviously be accounted for by the fact that our simple approach does not allow for the plethora of inelastic processes that occur in the real world; consequently our Argand plots stick too closely to the rim of the unitarity circle, and are simply much too large. Ideally one should allow for multiple-pion production, other mesons, and/or strangeness.

(2) The F-wave plots are in particularly close correspondence with experiment; this point has already been made in Ref. 12. Note that these are the first channels which do not mix with the zero-modes of the Skyrmion. In the F_{35} channel a speed-analysis actually revealed two overlapping resonances in the model at 1831 and 2032 MeV. Suggestively, the experimental data seem likewise characterized by a double peak, implying "that there might be additional structure, but the data do not allow additional structures to be resolved."[15] Consequently the assignment in the real world is to a single broad ($\Gamma=260\pm20$ MeV) F_{35} resonance at 1905 MeV. (Interestingly, a similar splitting of the F_{35} resonance is predicted by the quark model.[17])

(3) Even in those channels where the Argand diagrams

are not reproduced very well, the model accurately predicts the locations of resonances with an appropriate choice of e and f_π (see Table I). In fact, almost all of the masses are given to within 16% of their actual values, and a majority are given to 6%. This holds for all known resonances up to 3 GeV, which is surprising for a "low-energy" theory. The general rule that masses increase with increasing partial wave comes out naturally, while the model correctly pinpoints several exceptions to this rule in the lower waves.

(4) A serious discrepancy is that, except for P_{33}, the model fails to predict more than one resonance at reasonable energies in the channels where it should do so. In particular the model misses three 3- or 4-star resonances, namely, the $S_{11}(1650)$, $S_{31}(1900)$, and $D_{13}(1700)$, in addition of course to the Δ and the Roper resonance as we discussed at length.

(5) Except for the F and G waves, the model predicts widths that are too large by roughly 50% or more. (Question marks following some of our width assignments indicate a strong background phase shift to the right of the resonance which makes a precise determination of the widths difficult.) Note that, unlike the quark model, there is no particular reason in the Skyrme model why resonances should be narrow.[10]

(6) Finally, the Skyrme model makes a very strong prediction that, in each partial wave starting with the D wave, the $L_{1,2L-1}$ amplitude will move much further in the unitarity circle than the $L_{1,2L+1}$; while conversely, for the Δ-resonance channels, it is the $L_{3,2L+1}$ amplitude that dominates the $L_{3,2L-1}$. In addition this pattern is predicted to become substantially more pronounced with higher L. In fact, with a high degree of regularity, this is *precisely* what one finds in Nature, as a glance at the Argand plots confirms; the only arguable exceptions to the rule are the D- and I-wave Δ resonances. This important point is discussed in greater detail in Ref. 10.

Our results for the mass spectrum are presented in Table I. They are based on a least-squares fit with all resonances weighted equally. In fit 1 we fixed the proton mass, leaving only one free parameter, while in fit 2 we allowed the proton mass to vary. The optimal values for the Skyrme parameters turn out to be $\{e=6.29, f_\pi=142$ MeV$\}$ and $\{e=4.79, f_\pi=150$ MeV$\}$, respectively. An alternative approach would be to fix both the proton *and* the Δ mass using (5), which gives[4] $\{e=5.45, f_\pi=129$ MeV$\}$, but this yields a much poorer fit to the spectrum as a whole. (This is not too surprising since specifying the nucleon-Δ mass-difference involves a fine-tuning to order $1/N$.) In light of our earlier discussion we have chosen to compare the lowest-lying Skyrme-model excitations in the P_{11} and P_{33} channels, *not* with the physical Roper reso-

TABLE I. Comparison between experiment and Skyrme-model predictions for baryon resonances. Fit 1, nucleon mass fixed. Fit 2, nucleon mass allowed to vary.

Channel	Experiment	Fit 1	% error	Fit 2	% error
S_{11}	1526	1295	−15	1478	−3
S_{31}	1610	1295	−20	1478	−8
P_{11}	939	939	0	1190	27
P_{11}	1723	1233	−28	1427	−17
P_{13}	1710	1919	12	1982	16
P_{31}	1888	1919	2	1982	5
P_{33}	1232	1436	17	1424	16
P_{33}	1522	1242	−18	1435	−6
P_{33}	1868	1874	0.3	1946	4
D_{13}	1519	1589	5	1715	13
D_{15}	1679	1625	−3	1744	4
D_{33}	1680	1616	−4	1737	3
D_{35}	1901	1607	−15	1730	−9
F_{15}	1684	1723	2	1823	8
F_{17}	2005	1954	−3	2011	0.3
F_{35}	1905	1856[a]	−3	1931[b]	1
F_{37}	1913	1714	−10	1816	−5
G_{17}	2140	2034	−5	2075	−3
G_{19}	2268	2230	−2	2234	−2
G_{37}	2215	2141	−3	2162	−2
G_{39}	2468	2043	−17	2083	−16
H_{19}	2205	2346	6	2327	6
H_{39}	2217	2444	10	2407	9
$H_{3,11}$	2416	2346	−3	2327	−4
$I_{1,11}$	2577	2631	2	2558	−1
$I_{3,13}$	2794	2658	−5	2579	−8
$K_{1,13}$	2612	3032	16	2882	10
$K_{3,15}$	2990	2943	−2	2810	−6

[a]Average of two peaks at 1732 and 1981 MeV.
[b]Average of two peaks at 1831 and 2032 MeV.

nance and Δ, but with the next-higher resonances in those channels; our "predictions" in Table I for the Δ mass merely come from Eq. (5). In all other cases where there was more than one physical resonance in a channel we compared the Argand plots to determine which resonance we should actually use.

Note that fit 1 gives a nucleon-Δ mass difference that is much too large; in fact, it inverts the ordering of the first two P_{33} resonances. Furthermore the corresponding Skyrme parameters yield substantially worse *static* properties of the model when plugged into the formulas obtained in Ref. 4. For these reasons we prefer fit 2, which actually improves some of these properties, at the expense of allowing a proton mass of 1190 MeV [from Eq. (5)]; it is these mass assignments that we have noted in the Argand plots of Fig. 8.

Table II lists a handful of static properties that were first calculated[4] in the Skyrme model by Adkins, Nappi, and Witten (ANW). The middle column lists their predictions for the proton and neutron magnetic moments, the axial-vector coupling constant, and the mean isoscalar and isoscalar magnetic radii; the third column gives the same quantities recalculated[18] using the values for the Skyrme parameters given by fit 2; and the first column lists the experimental results. In summary, we find it intriguing that this simple two-parameter model could yield a reasonable fit to such a wide range of both static and dynamic properties of hadrons.

TABLE II. Static properties in the Skyrme model.

Quantity	Experiment	ANW	Fit 2
f_π	186 MeV	129 MeV	150 MeV
e	?	5.45	4.79
μ_p	2.79	1.87	2.83
μ_n	−1.91	−1.31	−2.29
g_A	1.23	0.61	0.79
$\langle r^2\rangle_{I=0}^{1/2}$	0.72 fm	0.59 fm	0.58 fm
$\langle r^2\rangle_{M,I=0}^{1/2}$	0.81 fm	0.92 fm	0.90 fm

ACKNOWLEDGMENTS

We would like to thank F. Gilman, M. Weinstein, and S. Yankielowicz for useful discussions. We are also grateful to Professor G. Höhler for providing us with his experimental results on pion-nucleon scattering. Our understanding of the experimental data has much benefited from conversations with David Leith. M.M. would like to thank Eric D'Hoker for arousing his interest in chiral solitons. Finally, we want to express our deep gratitude to Michael Peskin for his advice and constant support during all stages of this work. This work was supported by the Department of Energy, Contract No. DE-AC03-76F00515.

APPENDIX A: DETAILS CONCERNING DIFFERENTIAL EQUATIONS

In this appendix we give some further details concerning the differential equations (12a) and (12b). We will express our results in terms of the dimensionless variables $\tilde{r}=ef_\pi r$ and $\tilde{m}_\pi=m_\pi/ef_\pi$.

We consider the 1×1 case (12a) first. After multiplying through by $2F^2/\sin^2F$ the equation turns out to be

$$\left[1+\frac{4\sin^2F}{\tilde{r}^2}\right]\frac{d^2}{d\tilde{r}^2}\psi_0^K+\left[\frac{2}{\tilde{r}}+F'\left[2\cot F-\frac{2}{F}+\frac{8\sin2F}{\tilde{r}^2}-\frac{8\sin^2F}{F\tilde{r}^2}\right]\right]\frac{d}{d\tilde{r}}\psi_0^K$$

$$-\left[\frac{K(K+1)}{\tilde{r}^2}[1+4(F')^2]-\frac{2}{\tilde{r}^2}+F''\left[\frac{1}{F}+\frac{4\sin^2F}{\tilde{r}^2F}\right]+\frac{2F'}{\tilde{r}F}+(F')^2\left[-\frac{2}{F^2}-\frac{8\sin^2F}{\tilde{r}^2F^2}-\frac{8}{\tilde{r}^2}+\frac{2\cot F}{F}+\frac{8\sin2F}{\tilde{r}^2F}\right]\right.$$

$$\left.+\frac{F}{\tilde{r}^2\sin^2F}[\tilde{r}^2F''+\cdots]-\omega^2\left[1+4(F')^2+4\frac{\sin^2F}{\tilde{r}^2}\right]\right]\psi_0^K=0\ . \tag{A1}$$

The term $[\tilde{r}^2F''+\cdots]$ denotes the defining equation for F, Eq. (4), which of course is identically zero. Near the origin the regular solution satisfies

$$\psi_0^K\sim\tilde{r}^{K-1}[\pi-\alpha\tilde{r}+O(\tilde{r}^2)]\ ,$$

where $\alpha\equiv|F'(0)|\cong1$; from this we obtain the initial conditions needed to carry out the numerical integration. It is easily verified that the rotational mode (19a) solves (A1) when $K=1$ and $\omega=0$.

The 2×2 case (12b) is more complicated. It is convenient to change variables to

$$\psi_1^K=\frac{-K^{1/2}\psi_-^K+(K+1)^{1/2}\psi_+^K}{(2K+1)^{1/2}} \tag{A2a}$$

and

$$\psi_2^K=\frac{(K+1)^{1/2}\psi_-^K+K^{1/2}\psi_+^K}{(2K+1)^{1/2}}\ . \tag{A2b}$$

We then need to solve the coupled linear equations

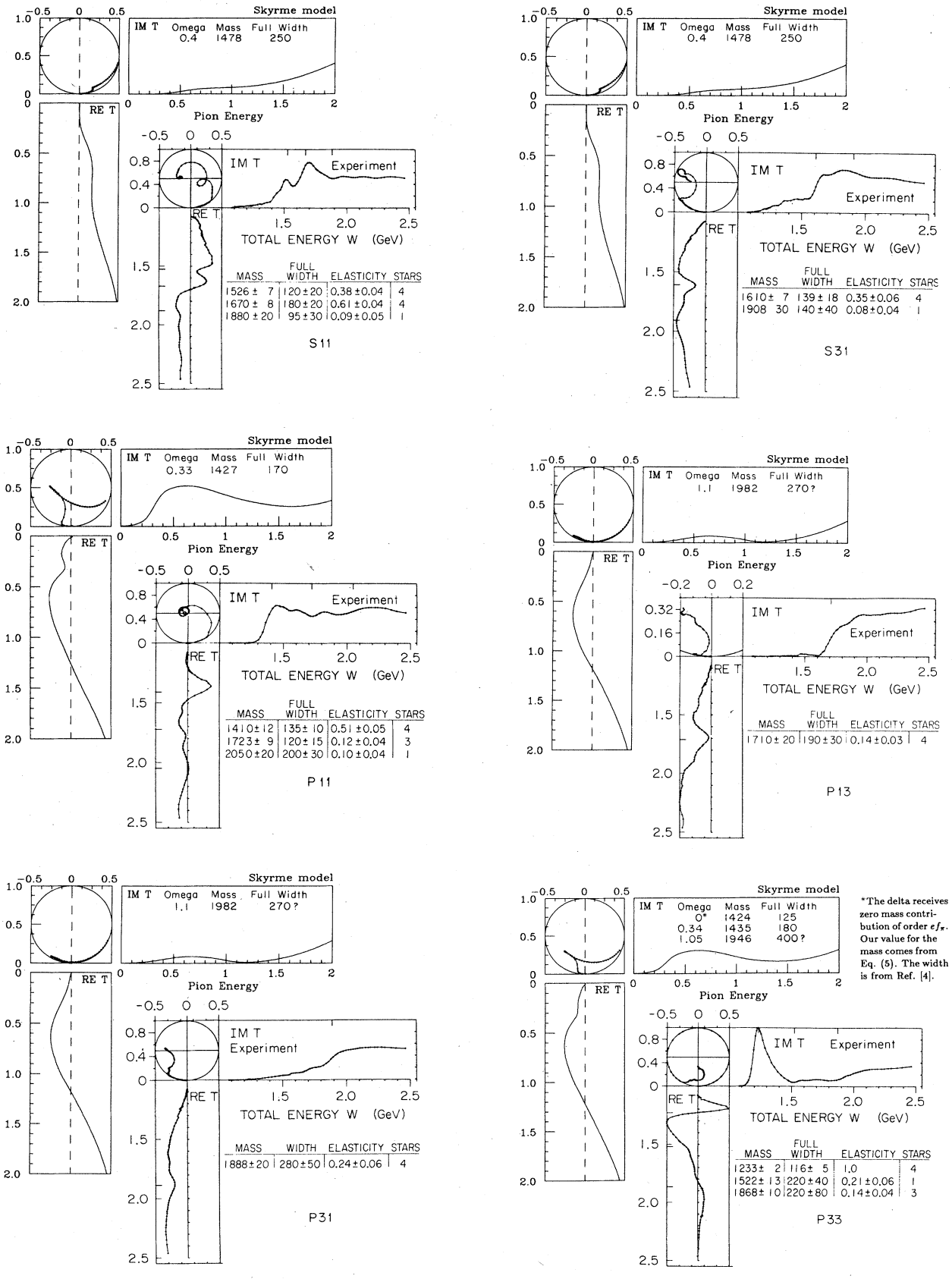

*The delta receives zero mass contribution of order $e f_\pi$. Our value for the mass comes from Eq. (5). The width is from Ref. [4].

FIG. 8. Experimental Argand plots (Ref. 15) for $\pi N \to \pi N$ juxtaposed with Skyrme-model results. See text (Appendix B).

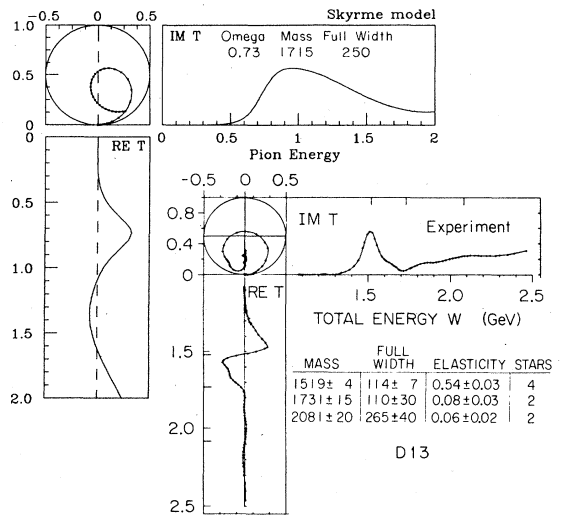

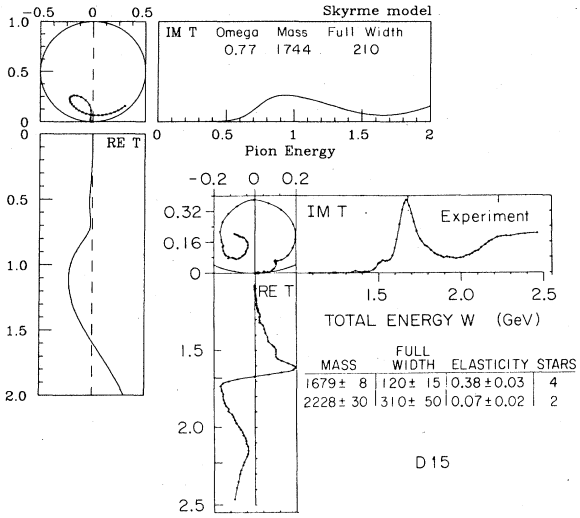

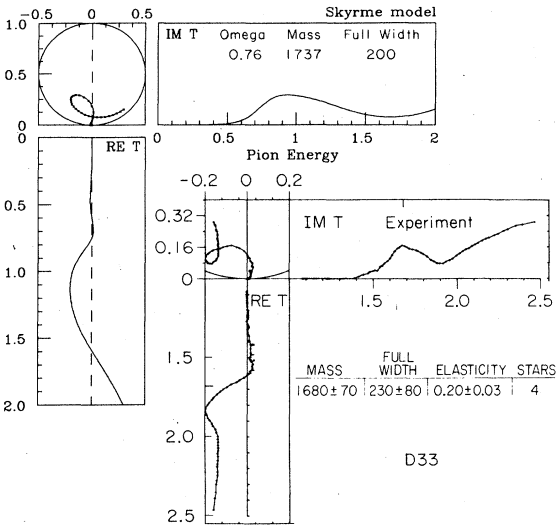

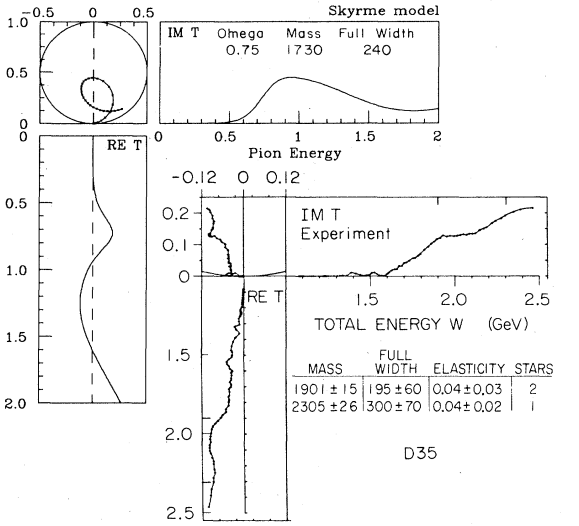

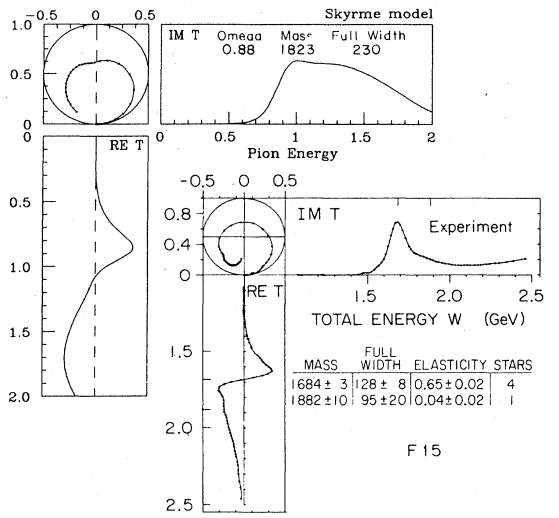

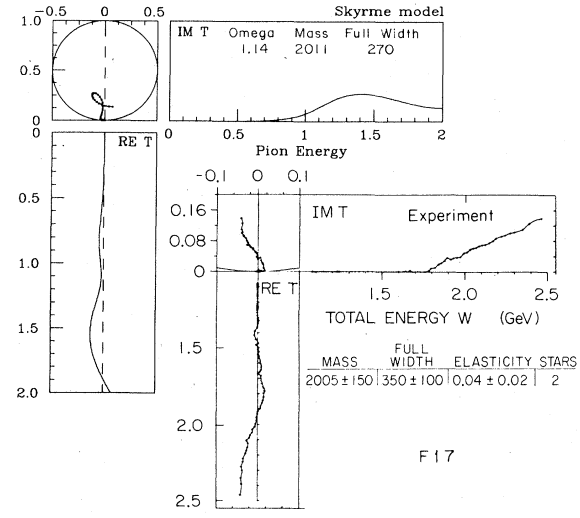

FIG. 8. (*Continued*).

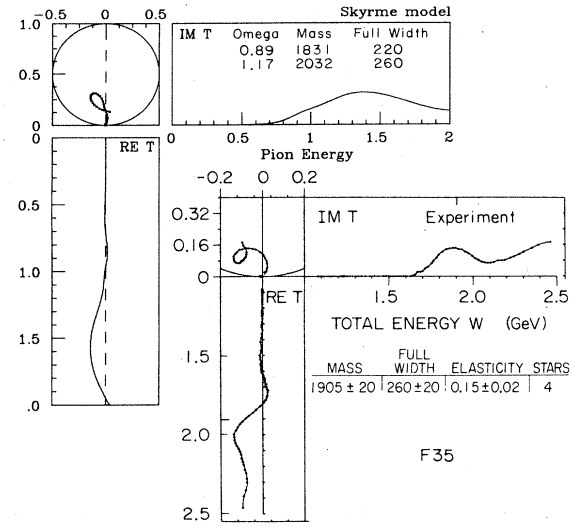

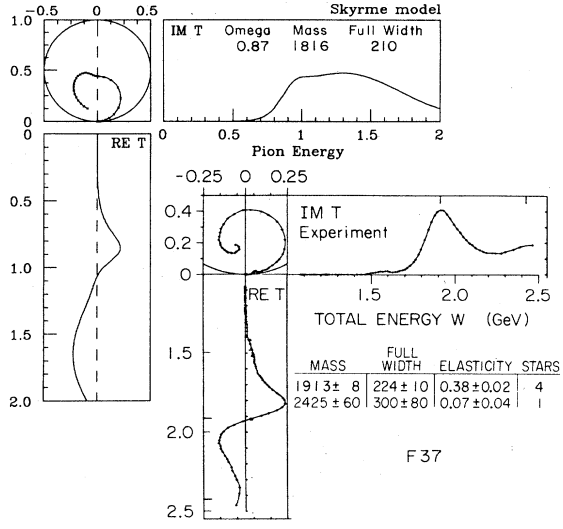

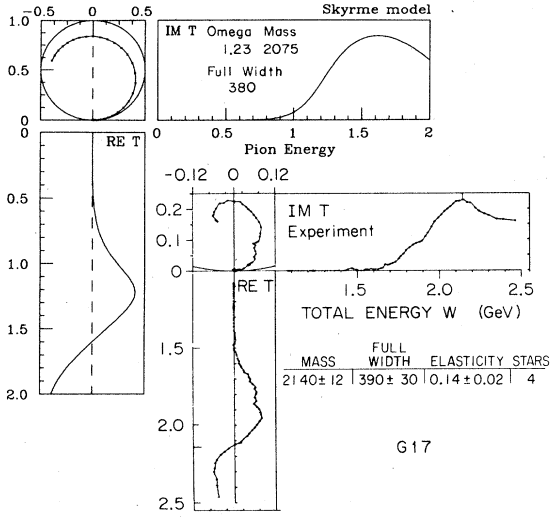

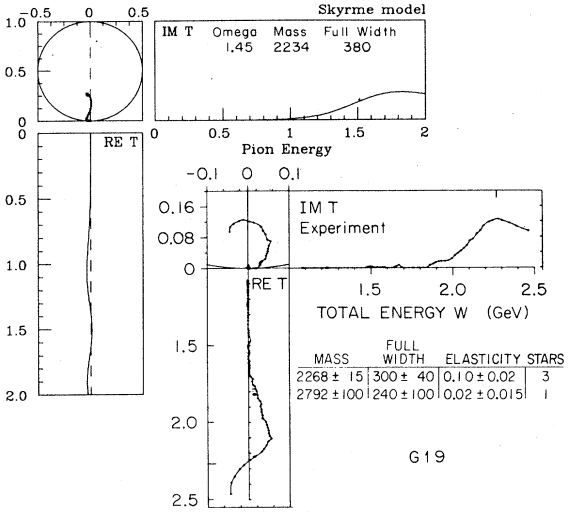

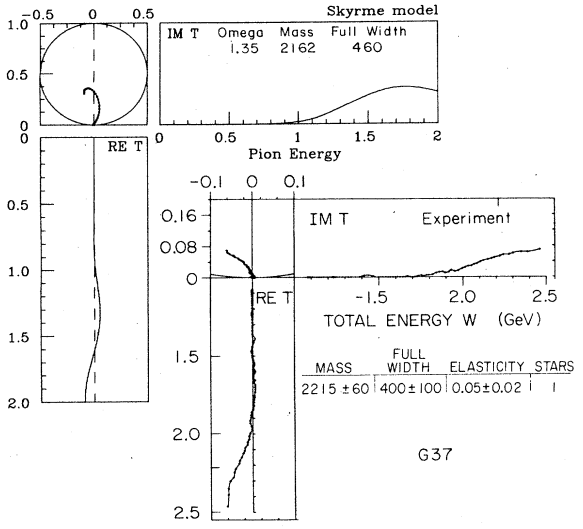

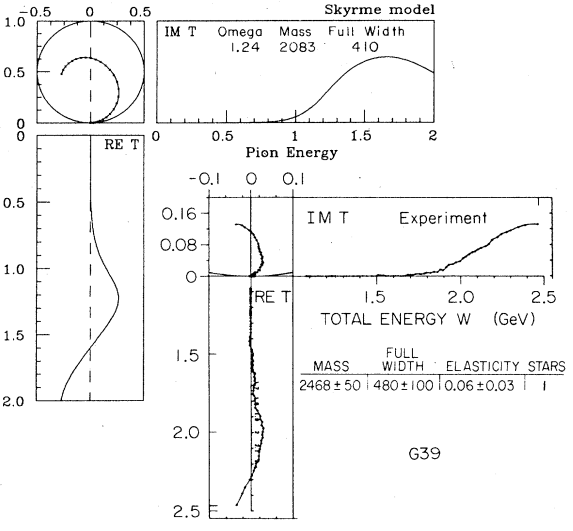

FIG. 8. (*Continued*).

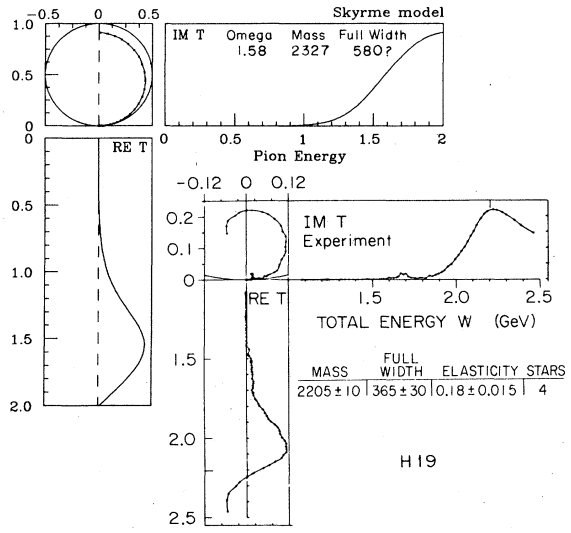

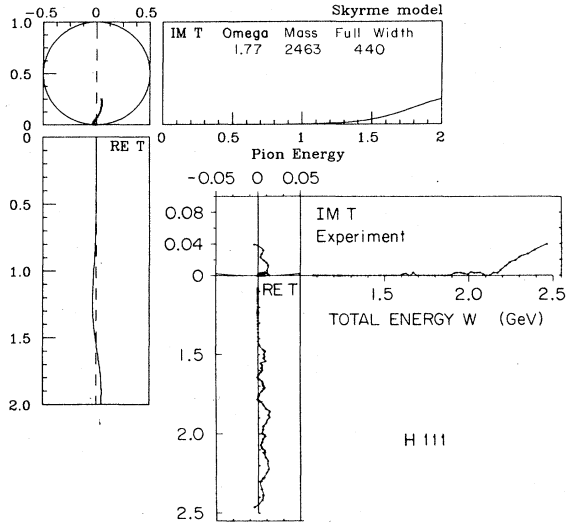

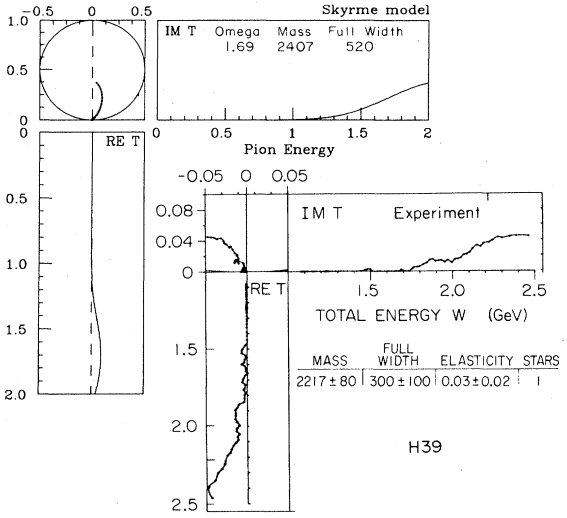

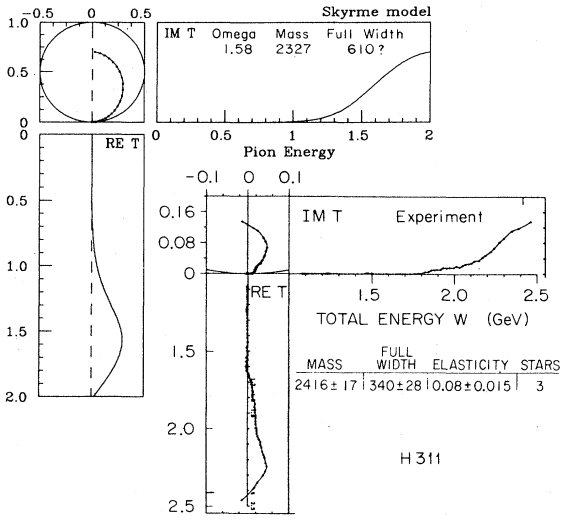

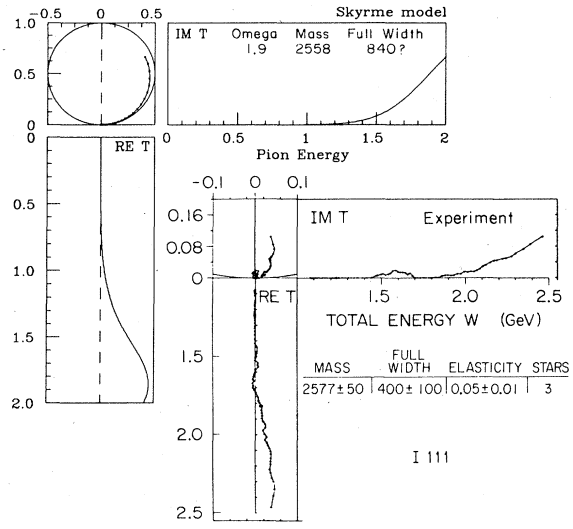

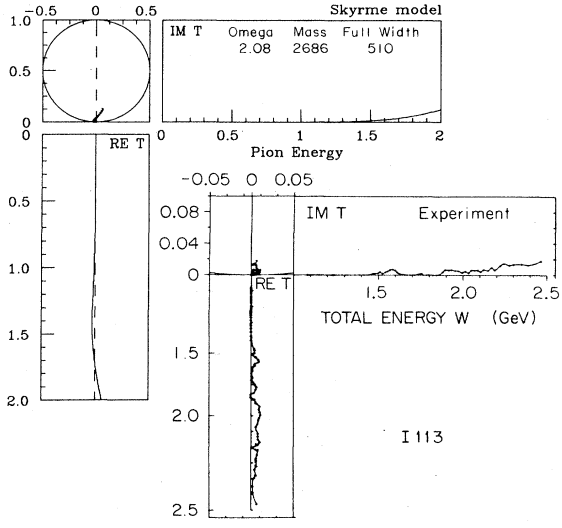

FIG. 8. (*Continued*).

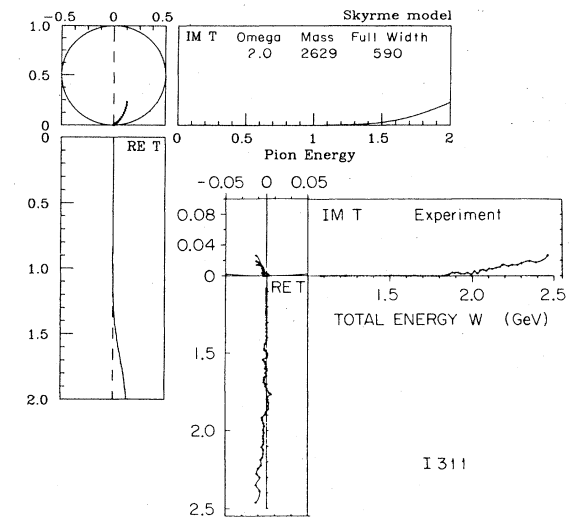

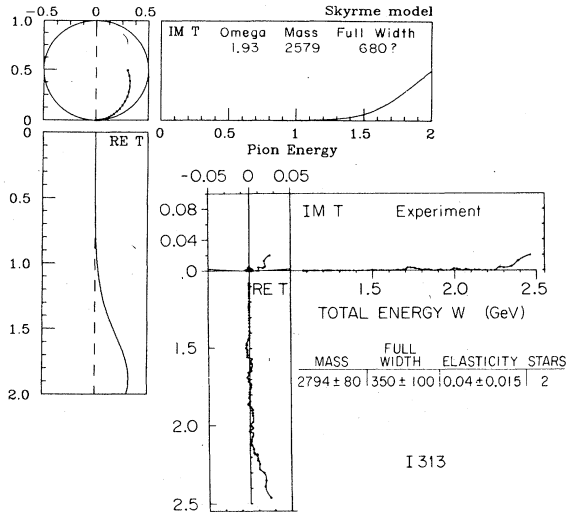

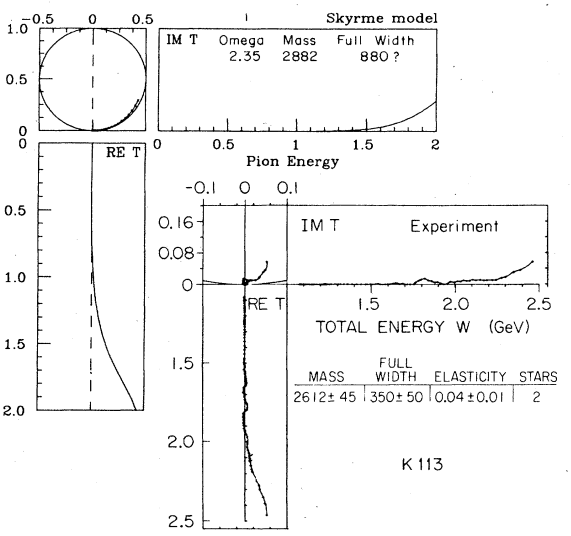

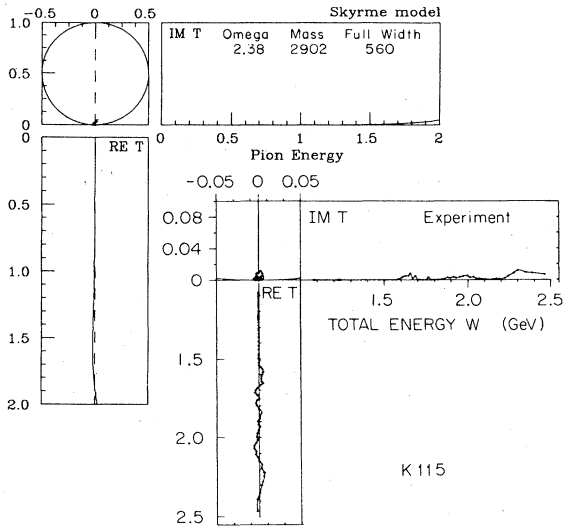

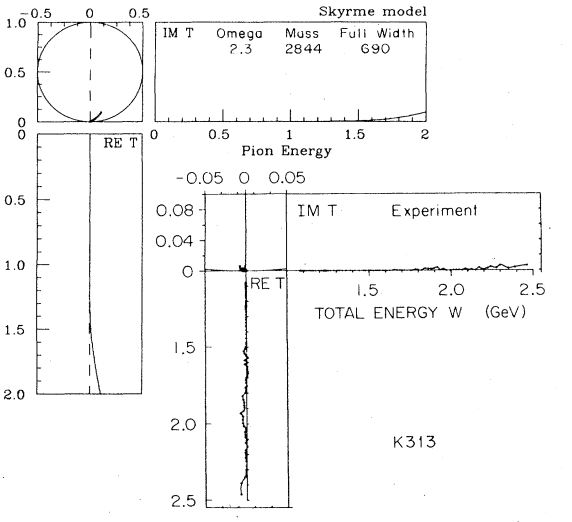

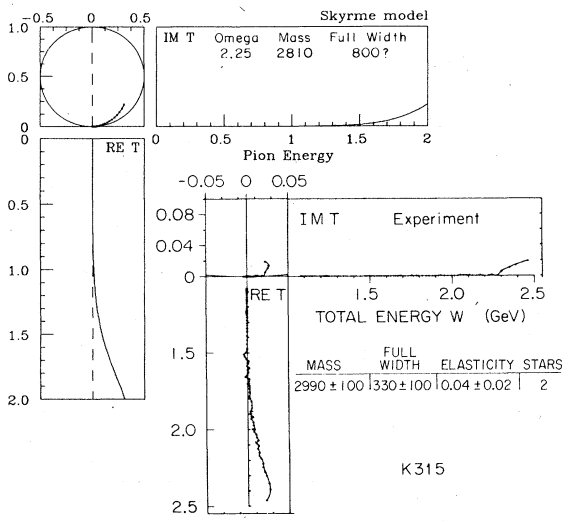

FIG. 8. (*Continued*).

$$-2F^4\tilde{r}^2(\tilde{r}^2+8\sin^2F)\frac{d^2}{d\tilde{r}^2}\psi_1^K-4F^4\tilde{r}^2(\tilde{r}+4F'\sin 2F)\frac{d}{d\tilde{r}}\psi_1^K$$
$$+\{2F^4[2\cos 2F+K(K+1)](\tilde{r}^2+4\sin^2F)+2F^4[4\sin^2 2F-8\tilde{r}^2F''\sin 2F+\tilde{m}_\pi^2\tilde{r}^4\cos F-8\tilde{r}^2(F')^2\cos 2F]$$
$$-2\tilde{r}^2F^4(\tilde{r}^2+8\sin^2F)\omega^2\}\psi_1^K-8[K(K+1)]^{1/2}F^3F'\tilde{r}^2\sin^2F\frac{d}{d\tilde{r}}\psi_2^K$$
$$+(F^2[K(K+1)]^{1/2}\sin^2F\{16F\sin 2F-16\tilde{r}^2FF''+4\tilde{r}^2F\cot F[1-4(F')^2]+8\tilde{r}^2(F')^2\}\psi_2^K=0 \quad \text{(A3a)}$$

and

$$-2F^2\tilde{r}^2(\tilde{r}^2+4\sin^2F)\frac{d^2}{d\tilde{r}^2}\psi_2^K+[-4F^2\tilde{r}^3+\tilde{r}^2F'(-16F^2\sin 2F-4F^2\cot F\tilde{r}^2+16F\sin^2F+4\tilde{r}^2F)]\frac{d}{d\tilde{r}}\psi_2^K$$
$$+\Big[K(K+1)F^2\{8\sin^2F+2\tilde{r}^2[1+4(F')^2]\}+2\tilde{r}^2[-8F^2(F')^2-2F^2+4F\sin^2FF''+8F\sin 2F(F')^2+F\tilde{r}(2F'+\tilde{r}F'')$$
$$+2F\cot F\tilde{r}^2(F')^2-8\sin^2F(F')^2-2\tilde{r}^2(F')^2]$$
$$-\frac{2\tilde{r}^2F^3}{\sin^2F}(\tilde{r}^2F''+\cdots)-2\omega^2F^2\tilde{r}^2[4\sin^2F+4\tilde{r}^2(F')^2+\tilde{r}^2]\Big]\psi_2^K$$
$$+8[K(K+1)]^{1/2}\tilde{r}^2F^3F'\frac{d}{d\tilde{r}}\psi_1^K+\{8F^3[K(K+1)]^{1/2}[2\sin 2F-\tilde{r}^2F''+\frac{\tilde{r}^2}{2}\cot F]\}\psi_1^K=0\,, \quad \text{(A3b)}$$

where we have multiplied through by $-4\tilde{r}^4F^4$ and $-4\tilde{r}^4F^4/\sin^2F$, respectively. (The advantage of the change of variables is that each of these equations is second order in only one variable.) We are relieved to find that, in the case of massless pions, Eqs. (A1) and (A3) are in agreement with Ref. 7. One can check that the translational mode (19b) is a zero-energy solution of Eq. (A3) when $K=1$.

For Eq. (A3) there are two regular solutions near the origin:

$$\begin{pmatrix}\psi_1^K\\ \psi_2^K\end{pmatrix}\sim\begin{pmatrix}\tilde{r}^{K\pm1}[1+O(\tilde{r}^2)]\\ B_\pm\tilde{r}^{K\pm1}\left[\frac{\pi}{\alpha\tilde{r}}-1+O(\tilde{r})\right]\end{pmatrix}, \quad \text{(A4)}$$

where

$$B_+=\left[\frac{K}{K+1}\right]^{1/2}\frac{1+2\alpha^2K+10\alpha^2}{-1+2\alpha^2K-4\alpha^2}$$

and

$$B_-=\left[\frac{K+1}{K}\right]^{1/2}.$$

It is straightforward to integrate these equations numerically out to large $\tilde{r}$, reconstruct $\psi_\pm^K$, and extract the phase shifts. The development then proceeds as outlined in Sec. II.

APPENDIX B: ARGAND PLOTS FOR ELASTIC πN SCATTERING: SKYRME MODEL VS EXPERIMENT

In Fig. 8 we present the experimental Argand plots[15] for $\pi N\to\pi N$ juxtaposed with the Skyrme-model results. (In each pair these are the "inner" and "outer" graphs, respectively.) Both the experimental and the Skyrme-model plots consist of three parts: Imaginary vs real part of the scattering amplitude T, imaginary part of T vs energy, and real part of T vs energy.

In the Skyrme-model plots, the energy in question is pion energy ω, which is given in units of ef_π. Resonance masses are given in terms of this unit, as well as in MeV, (using our best-fit value $ef_\pi=718.5$ MeV); full widths are given only in MeV. The experimental graphs are parametrized by *total* energy in MeV, and masses and widths are likewise in MeV.

[1]T. H. R. Skyrme, Proc. R. Soc. London **A260**, 127 (1961).
[2]E. Witten, Nucl. Phys. **B160**, 57 (1979).
[3]E. Witten, Nucl. Phys. **B223**, 422 (1983); **B223**, 433 (1983).
[4]G. S. Adkins, C. R. Nappi, and E. Witten, Nucl. Phys. **B228**, 552 (1983). For an update on recent developments see *Proceedings of the Lewes Workshop on Solitons in Nuclear and Elementary Particle Physics, 1984,* edited by A. Chodos, E. Hadjimichael, and C. Tze (World Scientific, Singapore, 1984).
[5]I. Zahed, U.-G. Meissner, and U. B. Kaulfuss, Nucl. Phys. **A426**, 525 (1984).
[6]J. D. Breit and C. R. Nappi, Phys. Rev. Lett. **53**, 889 (1984).
[7]H. Walliser and G. Eckart, Nucl. Phys. **A429**, 514 (1984).
[8]The breathing mode is also discussed in C. Hajduk and B. Schwesinger, Phys. Lett. **140B**, 172 (1984); J. Dey and J. Le Tourneux, Montreal report, 1984 (unpublished); J. D. Breit,

Phys. Lett. B (to be published); K. F. Liu, J. S. Zhang, and G. R. E. Black, Phys. Rev. D **30**, 2015 (1984); A. Parmentola, *ibid.* **30**, 685 (1984); L. C. Biedenharn, Y. Dothan, and M. Tarlini, *ibid.* **31**, 649 (1985). See also Refs. 11 and 12.

[9]M. Karliner and M. Mattis (in preparation).

[10]M. Mattis and M. Peskin, Phys. Rev. D (to be published).

[11]A. Hayashi and G. Holzwarth, Phys. Lett. **140B**, 175 (1984).

[12]A. Hayashi, G. Eckart, G. Holtzwarth, and H. Walliser, Phys. Lett. **147B**, 5 (1984).

[13]M. Messiah, *Quantum Mechanics* (North-Holland, Amsterdam, 1961).

[14]See, for example, J. R. Taylor, *Scattering Theory* (Wiley, New York, 1972).

[15]G. Höhler, F. Kaiser, R. Koch, and E. Pietarinen, *Handbook of Pion-Nucleon Scattering,* Physics Data No. 12-1 (Fachsinformationszentrum, Karlsruhe, 1979).

[16]In light of our "no-recoil" approach, which is not only built into our treatment of pion scattering in the *fixed* Skyrmion background but also implicit in the derivation of Eq. (20), we interpret the rest mass of a resonance to be given simply by the sum $m_N+\omega$; this is in accord with Ref. 6.

[17]N. Isgur and G. Karl, Phys. Rev. D **18**, 4187 (1978); **19**, 2653 (1979); **20**, 1191 (1979).

[18]The values of μ_p and μ_n given in the third column of Table II are in units of the Bohr magneton obtained from $m_p=1190$ MeV. In units of the *physical* Bohr magneton one obtains instead: $\mu_p 2.23$, $\mu_n=-1.81$.